Int J Fract (2007) 145:313–326
DOI 10.1007/s10704-007-9130-1

ORIGINAL PAPER

Evaluation of fracture parameters in continuously nonhomogeneous piezoelectric solids

Jan Sladek · V. Sladek · Ch. Zhang · P. Solek · E. Pan

Received: 14 May 2007 / Accepted: 21 September 2007 / Published online: 16 October 2007

Abstract A contour integral method is developed for computation of stress intensity and electric intensity factors for cracks in continuously nonhomogeneous piezoelectric body under a transient dynamic load. It is shown that the asymptotic fields in the crack-tip vicinity in a continuously nonhomogeneos medium is the same as in a homogeneous one. A meshless method based on the local Petrov-Galerkin approach is applied for computation of physical fields occurring in the contour integral expressions of intensity factors. A unit step function is used as the test functions in the local weak-form. This leads to local integral equations (LBIEs) involving only contour-integrals on the surfaces of subdomains. The moving least-squares (MLS) method is adopted for approximating the physical quantities in the LBIEs. The accuracy of the present method for computing the stress intensity factors (SIF) and electrical displacement intensity factors (EDIF) are discussed by comparison with available analytical or numerical solutions.

Keywords Meshless local Petrov-Galerkin method (MLPG) · Moving least-squares interpolation · Piezoelectric solids · Functionally graded materials · Intensity factors · Dynamic loading

J. Sladek (✉) · V. Sladek
Institute of Construction and Architecture, Slovak Academy of Sciences, 84503 Bratislava, Slovakia
e-mail: usarslad@savba.sk

Ch. Zhang
Department of Civil Engineering, University of Siegen, 57068 Siegen, Germany

P. Solek
Department of Mechanics, Slovak Technical University, Bratislava, Slovakia

E. Pan
Computer Modeling and Simulation Group, Department of Civil Engineering, University of Akron, Akron, OH, 44325-3905, USA

1 Introduction

Functionally graded materials (FGMs) have demonstrated that they have a potential to reduce the stress concentration and increase the fracture toughness (Suresh and Mortensen 1998; Paulino et al. 2003). Consequently, the concept of FGMs can be extended to the piezoelasticity to obtain piezoelectric materials with high strength, high toughness, low thermal expansion coefficient and low dielectric constant. Devices such as actuators based on functionally graded piezoelectric materials (FGPMs) were given by Zhu et al. (1995, 1999) and Han et al. (2006). The fracture of FGPMs under a thermal load has been studied by Wang and Noda (2001). An anti-plane crack problem is described by relatively simpler governing equations than for in-plane problems (Li and Weng 2002a). The problem of a functionally piezoelectric graded material with Yoffe-type moving crack of a constant-velocity is analyzed by Li and Weng (2002b). Recently, the in-plane crack problem in FGPMs has been analyzed by

Chen et al. (2003) and Ueda (2003). To the best of the authors' knowledge, only one paper (Chen et al. 2002) is devoted to three-dimensional (3D) electroelastic fields in FGPMs.

The solution of the boundary value problems for continuously nonhomogeneous piezoelectric solids requires advanced numerical methods due to the high mathematical complexity. The governing equations are more complicated than in a homogeneous counterpart and the electric and mechanical fields are coupled each other. Therefore, a variety of different crack problems in piezoelectric medium have been studied in homogeneous or multi-layered bodies. Pak (1990) obtained the closed form solutions for an infinite piezoelectric medium under an anti-plane loading by using a complex variable method. Later, Park and Sun (1995) obtained closed form solutions for all three fracture modes for a crack in an infinite medium. They investigated the effects of the electric field on the fracture of piezoelectric ceramics. Shindo et al. (1996, 1997) used an integral transform method to analyze a crack in an infinite strip. Yang and Lee (2001) applied the same method for a penny shaped crack in a three-dimensional piezoelectric strip under in-plane normal loading. The dual integral equations approach used in the above mentioned papers is restricted to problems with a simple geometry and boundary conditions. Modern computational methods like the finite element method (FEM) (Gruebner et al. 2003; Govorukha and Kamlah 2004; Enderlein et al. 2005; Kuna 1998, 2006) and the boundary element method (BEM) (Pan 1999; Davi and Milazzo 2001; Gross et al. 2005; Garcia–Sanchez et al. 2005, 2007; Sheng and Sze 2006) have to be applied for general crack analyses in piezoelectric solids.

In spite of the great success on these effective numerical tools for the solution of boundary value problems in piezoelectric solids, there is still a growing interest in the development of new advanced methods. In recent years, meshless formulations are becoming popular due to their high adaptivity and low costs to prepare input and output data for numerical analyses. A variety of meshless methods has been proposed so far and some of them also applied to piezoelectric problems (Ohs and Aluru 2001; Liu et al. 2002). They can be derived either from a weak-form formulation on the global domain or a set of local subdomains. In the global formulation, background cells are required for the integration of the weak-form. In the methods based on the local weak-form formulation no background cells are required and therefore they are often referred to as truly meshless methods. The meshless local Petrov-Galerkin (MLPG) method is a fundamental base for the derivation of many meshless formulations, since trial and test functions can be chosen from different functional spaces. Recently, the MLPG method with a Heaviside step function as the test functions (Atluri et al. 2003, 2006; Atluri 2004; Sladek et al. 2004) has been applied to solve two-dimensional (2D) homogeneous piezoelectric problems by the authors (Sladek et al. 2006). In the present paper, the MLPG is extended to continuously nonhomogeneous solids with cracks under a transient dynamic load. The coupled governing partial differential equations are satisfied in a weak-form on small fictitious subdomains. Nodal points are introduced and spread on the analyzed domain and each node is surrounded by a small circle for simplicity, but without loss of generality. If the shape of subdomains has a simple form, numerical integrations over them can be easily carried out. The integral equations have a very simple nonsingular form. The spatial variations of the displacements and the electric potential are approximated by the Moving Least-Squares (MLS) scheme (Belytschko et al. 1996; Zhu et al. 1998). After performing the spatial integrations, a system of linear algebraic equations for unknown nodal values is obtained. The boundary conditions on the global boundary are satisfied by the collocation of the MLS-approximation expressions for the displacements and the electric potential at the boundary nodal points. A contour integral method is developed for the computation of the stress intensity and electric intensity factors for cracks in continuously nonhomogeneous piezoelectric solids under a transient dynamic load. It is shown that the asymptotic fields in the crack tip vicinity in a continuously nonhomogeneos medium is the same as in a homogeneous one.

2 Asymptotic fields in the crack tip vicinity in FGM

The governing equations for continuously nonhomogeneous piezoelectric solids are given by the equations of motion for the mechanical displacements and by the first Maxwell equation for the vector of electric displacements (Parton and Kudryavtsev 1988)

$$\sigma_{ij,j} + X_i = \rho \ddot{u}_i, \tag{1}$$

$$D_{j,j} - R = 0, \tag{2}$$

where $\ddot{u}_i$, σ_{ij}, D_i, X_i, R and ρ denote the acceleration, stress tensor, electric displacement, body force vector, volume density of free charges and mass density, respectively.

The constitutive relations represent the coupling of the mechanical and the electrical fields. They can be obtained as derivatives of the electric enthalpy density $W = W(\varepsilon_{ij}, E_i, x_i)$ (Parton and Kudryavtsev 1988) in the following manner

$$\begin{aligned} W(\varepsilon_{ij}, E_i, \mathbf{x}) = &\frac{1}{2} c_{ijkl}(\mathbf{x})\varepsilon_{ij}(\mathbf{x})\varepsilon_{kl}(\mathbf{x}) \\ &- e_{ikl}(\mathbf{x})E_i(\mathbf{x})\varepsilon_{kl}(\mathbf{x}) \\ &- \frac{1}{2} h_{ij}(\mathbf{x})E_i(\mathbf{x})E_j(\mathbf{x}), \end{aligned} \tag{3}$$

$$\sigma_{ij}(\mathbf{x}) = \frac{\partial W}{\partial \varepsilon_{ij}} = c_{ijkl}(\mathbf{x})\varepsilon_{kl}(\mathbf{x}) - e_{kij}(\mathbf{x})E_k(\mathbf{x}), \tag{4}$$

$$D_j(\mathbf{x}) = -\frac{\partial W}{\partial E_j} = e_{jkl}(\mathbf{x})\varepsilon_{kl}(\mathbf{x}) + h_{jk}(\mathbf{x})E_k(\mathbf{x}), \tag{5}$$

where $c_{ijkl}(\mathbf{x})$, $e_{jkl}(\mathbf{x})$and $h_{jk}(\mathbf{x})$are the elastic, piezoelectric and dielectric material tensors in a continuously nonhomogeneous piezoelectric medium, respectively. The strain tensor ε_{ij} and the electric field vector E_j are related to the displacements u_i and the electric potential ψ by

$$\varepsilon_{ij} = \frac{1}{2}\left(u_{i,j} + u_{j,i}\right), \tag{6}$$

$$E_j = -\psi_{,j}. \tag{7}$$

In this analysis, we assume that the piezoelectric solids are transversely isotropic with $\varepsilon_{33} = \varepsilon_{31} = \varepsilon_{32} = E_3 = 0$ (i.e., we apply the plane strain conditions). In such a case, the constitutive Eqs. 4 and 5 are reduced to (Sheng and Sze 2006)

$$\begin{bmatrix} \sigma_{11} \\ \sigma_{22} \\ \sigma_{12} \end{bmatrix} = \begin{bmatrix} c_{11} & c_{12} & 0 \\ c_{12} & c_{22} & 0 \\ 0 & 0 & c_{44} \end{bmatrix} \begin{bmatrix} \varepsilon_{11} \\ \varepsilon_{22} \\ 2\varepsilon_{12} \end{bmatrix} - \begin{bmatrix} 0 & e_{21} \\ 0 & e_{22} \\ e_{15} & 0 \end{bmatrix} \times \begin{bmatrix} E_1 \\ E_2 \end{bmatrix} = \mathbf{C}(\mathbf{x}) \begin{bmatrix} \varepsilon_{11} \\ \varepsilon_{22} \\ 2\varepsilon_{12} \end{bmatrix} - \mathbf{L}(\mathbf{x}) \begin{bmatrix} E_1 \\ E_2 \end{bmatrix}, \tag{8}$$

$$\begin{bmatrix} D_1 \\ D_2 \end{bmatrix} = \begin{bmatrix} 0 & 0 & e_{15} \\ e_{21} & e_{22} & 0 \end{bmatrix} \begin{bmatrix} \varepsilon_{11} \\ \varepsilon_{22} \\ 2\varepsilon_{12} \end{bmatrix} + \begin{bmatrix} h_{11} & 0 \\ 0 & h_{22} \end{bmatrix} \times \begin{bmatrix} E_1 \\ E_2 \end{bmatrix} = \mathbf{G}(\mathbf{x}) \begin{bmatrix} \varepsilon_{11} \\ \varepsilon_{22} \\ 2\varepsilon_{12} \end{bmatrix} + \mathbf{H}(\mathbf{x}) \begin{bmatrix} E_1 \\ E_2 \end{bmatrix}. \tag{9}$$

Let us extract the crack tip values of the material parameters as

$$\begin{aligned} c_{ijkl}(\mathbf{x}) &= c^0_{ijkl} + \tilde{c}_{ijkl}(\mathbf{x}), \\ e_{kij}(\mathbf{x}) &= e^0_{kij} + \tilde{e}_{kij}(\mathbf{x}), \\ h_{ij}(\mathbf{x}) &= h^0_{ij} + \tilde{h}_{ij}(\mathbf{x}). \end{aligned} \tag{10}$$

Then, the perturbations, denoted by wave, behave like $O(r)$, where $r$is the distance of the observation point $\mathbf{x}$ from the crack tip.

The governing equations involve the gradients of stresses and electrical displacements which are given in a medium with continuously varying material properties as

$$\begin{aligned} \sigma_{ij,j} &= c_{ijkl}u_{k,lj} - e_{kij}E_{k,j} + c_{ijkl,j}u_{k,l} - e_{kij,j}E_k, \\ D_{j,j} &= e_{jkl}u_{k,lj} + h_{ji}E_{i,j} + e_{jkl,j}u_{k,l} + h_{ji,j}E_i. \end{aligned} \tag{11}$$

For analyzing the asymptotic fields in the crack tip vicinity, the body forces and volume charges are assumed to be zero. Utilizing Eq. 10 in a quasi-static case, one obtains from (1) and (2)

$$\begin{aligned} c^0_{ijkl}u_{k,lj} - &\; e^0_{kij}E_{k,j} + \tilde{c}_{ijkl}u_{k,lj} - \tilde{e}_{kij}E_{k,j} \\ &+ c_{ijkl,j}u_{k,l} - e_{kij,j}E_k = 0, \end{aligned} \tag{12}$$

$$\begin{aligned} e^0_{ikl}u_{k,lj} &+ h^0_{ji}E_{i,j} + \tilde{e}_{ikl}u_{k,lj} + \tilde{h}_{ji}E_{i,j} \\ &+ e_{jkl,j}u_{k,l} + h_{ji,j}E_i = 0. \end{aligned} \tag{13}$$

Separation of variables method in polar coordinate system is appropriate to solve Eqs. 12 and 13. Our aim is to show that the asymptotic fields in continuously nonhomogeneous medium are the same as in a homogeneous one. For this purpose we assume that in the near vicinity of the crack tip, the mechanical displacement variation with the radial coordinate as $u_i \sim r^\lambda$, where λ is an unspecified positive parameter. From the governing Eq. 2 and the constitutive Eq. 5, one can find directly that the electric field behaves like$E_i \sim r^{\lambda-1}$. Then, taking into account the asymptotic behaviour of the material parameters in continuously non-homogeneous medium in accordance with Eq. 10, we can rewrite Eqs. 12 and 13 into the form

$$c^0_{ijkl}u_{k,lj} - e^0_{kij}E_{k,j} + O(r^{\lambda-1}) = 0, \tag{14}$$

$$e^0_{ikl}u_{k,lj} + h^0_{ji}E_{i,j} + O(r^{\lambda-1}) = 0. \tag{15}$$

Thus, the leading singularity is determined by the following equations

$$c^0_{ijkl}u_{k,lj} - e^0_{kij}E_{k,j} = 0, \tag{16}$$

$$e^0_{ikl}u_{k,lj} + h^0_{ji}E_{i,j} = 0, \tag{17}$$

which are valid for a homogeneous body with material constants given by the crack tip values of the corresponding material parameters in the considered nonhomogeneous medium. Similar approach has been used by Jin and Noda (1994) to show the dominant crack-tip singularity in a continuously nonhomogeneous body in elasticity. The nature of the stress singularity is precisely the same as well-known form applicable to homogeneous materials (Eischen 1987).

For cracks in homogeneous piezoelectric media the asymptotic behaviour of the field quantities has been given by Sosa (1991) and Pak (1992). If polar coordinates $(r, \theta)$with the origin at the crack tip are used, the electromechanical fields can be written as

$$\begin{aligned} \sigma_{ij}(r,\theta) &= \frac{1}{\sqrt{2\pi r}}\sum_{N=1}^{4} K_N f^N_{ij}(\theta), \\ D_i(r,\theta) &= \frac{1}{\sqrt{2\pi r}}\sum_{N=1}^{4} K_N g^N_i(\theta) \end{aligned} \tag{18}$$

$$\begin{aligned} u_i(r,\theta) &= \sqrt{\frac{2r}{\pi}}\sum_{N=1}^{4} K_N d^N_i(\theta), \\ \psi(r,\theta) &= \sqrt{\frac{2r}{\pi}}\sum_{N=1}^{4} K_N \nu^N(\theta), \end{aligned} \tag{19}$$

where K_I, K_{II} and K_{III} denote the well-known mechanical stress intensity factors (SIF) and $K_{IV}$is the electrical displacement intensity factor (EDIF). The angular functions $f^N_{ij}(\theta)$, $g^N_i(\theta)$, $d^N_i(\theta)$ and $\nu^N(\theta)$ are dependent on material properties only and given by

$$f^N_{i1} = -\sum_{\alpha=1}^{4} Re\left\{\frac{M_{i\alpha}N_{\alpha N}p_\alpha}{\sqrt{\cos\theta + p_\alpha \sin\theta}}\right\},$$

$$f^N_{i2} = \sum_{\alpha=1}^{4} Re\left\{\frac{M_{i\alpha}N_{\alpha N}}{\sqrt{\cos\theta + p_\alpha \sin\theta}}\right\},$$

$$g^N_1 = -\sum_{\alpha=1}^{4} Re\left\{\frac{M_{4\alpha}N_{\alpha N}p_\alpha}{\sqrt{\cos\theta + p_\alpha \sin\theta}}\right\},$$

$$g^N_2 = \sum_{\alpha=1}^{4} Re\left\{\frac{M_{4\alpha}N_{\alpha N}}{\sqrt{\cos\theta + p_\alpha \sin\theta}}\right\},$$

$$d^N_i = \sum_{\alpha=1}^{4} Re\left\{A_{i\alpha}N_{\alpha N}\sqrt{\cos\theta + p_\alpha \sin\theta}\right\},$$

$$\nu^N = \sum_{\alpha=1}^{4} Re\left\{A_{4\alpha}N_{\alpha N}\sqrt{\cos\theta + p_\alpha \sin\theta}\right\},$$

where $p_\alpha$are eigenvalues of the characteristic equations for an anisotropic body and the matrices $A_{i\alpha}$, $M_{i\alpha}$and $N_{\alpha N}$are defined in the work (Park and Sun 1995). The asymptotic expressions (18) and (19) are used in the next paragraph as auxiliary fields. From Eq. 19 one can derive expression for the mode-I SIF,K_I, in terms of the near-field displacement and the electrical potential (Ricoeur and Kuna 2003)

$$K_I = \lim_{r\to 0}\sqrt{\frac{\pi}{2r}}\left(\frac{c_T e^2}{c_T\kappa + e^2}u_2 + \frac{c_T\kappa}{c_T\kappa + e^2}\psi\right), \tag{20}$$

where c_T, e and κ are the effective material constants of the simplified Irwin matrix (Kuna 2006)

$$Y_{MN} = -\sum_{\alpha=1}^{4} Re\{A_{M\alpha}N_{\alpha N}\}.$$

3 Evaluation of the intensity factors in FGM

The gradient of the electric enthalpy density (3) is given as

$$W_{,m}(\varepsilon_{ij}, E_n, x_i) = \frac{\partial W}{\partial \varepsilon_{ij}}\frac{\partial \varepsilon_{ij}}{\partial x_m} + \frac{\partial W}{\partial E_n}\frac{\partial E_n}{\partial x_m} + \left(\frac{\partial W}{\partial x_m}\right)_{\exp l}, \tag{21}$$

where the term for the "explicit" derivative of the enthalpy density for non-homogeneous materials becomes

$$\left(\frac{\partial W}{\partial x_m}\right)_{\exp l} = \frac{1}{2}c_{ijkl,m}\varepsilon_{ij}\varepsilon_{kl} - e_{ikl,m}E_i\varepsilon_{kl} - \frac{1}{2}h_{ij,m}E_iE_j. \tag{22}$$

Then, utilizing Eqs. 4, 5 and 6, the gradient of the strain energy density can be rewritten into the form

$$W_{,m} = \left(\sigma_{ij}u_{i,m}\right)_{,j} - \sigma_{ij,j}u_{i,m} - D_nE_{n,m} + (W_{,m})_{\exp l}. \tag{23}$$

Bearing in mind Eq. 7, one can write the third term in Eq. 23 as

$$D_nE_{n,m} = D_nE_{m,n} = (D_nE_m)_{,n} - D_{n,n}E_m.$$

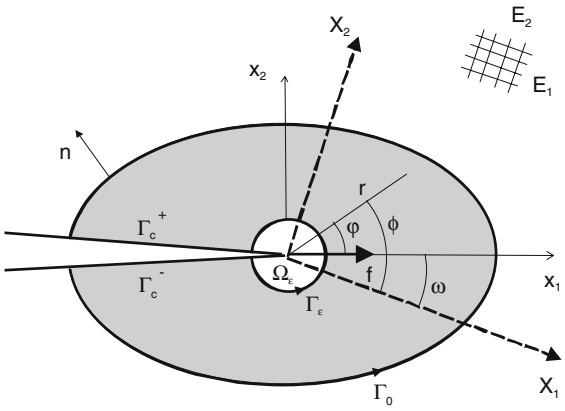

Fig. 1 Integration paths and coordinate definitions

Then, the gradient of the electric enthalpy density is given as

$$\left(W\delta_{jm} - \sigma_{ij}u_{i,m} - D_j E_m\right)_{,j} = \left(X_i - \rho\ddot{u}_i\right)u_{i,m} - RE_m + (W_{,m})_{\exp l}\,. \tag{24}$$

An integral form of Eq. 24 may be obtained upon application of the divergence theorem. If Ω is a regular bounded region enclosed by a surface Γ whose unit outward normal vector is $\mathbf{n}$, it follows that

$$\int_{\Gamma}\left(W\delta_{jm} - \sigma_{ij}u_{i,m} - D_j E_m\right)n_j \mathrm{d}\Gamma = \int_{\Omega}\left(X_i - \rho\ddot{u}_i\right)u_{i,m}\mathrm{d}\Omega - \int_{\Omega} RE_m \mathrm{d}\Omega + \int_{\Omega}(W_{,m})_{\exp l}\,\mathrm{d}\Omega. \tag{25}$$

The integral identity (25) is valid in a region where no field irregularities prevail. In the presence of a crack, the stresses at the crack-tip are singular and the displacements are discontinuous across both crack-surfaces. Therefore, a cut-off along the crack with a small region at the vicinity of a crack-tip Ω_ε has to be excluded. This region is surrounded by Γ_ε as shown in Fig. 1.

The global Cartesian coordinate system is defined in such a way that the principal axes of the material orthotropy are aligned with the global coordinates. All fields σ_{ij}, u_i, D_j and E_j are regular in the region $\Omega - \Omega_\varepsilon$. The contour $\Gamma = \Gamma_0 + \Gamma_c^+ - \Gamma_\varepsilon + \Gamma_c^-$ is a closed integration path in the counter-clockwise direction. The radius ε is considered to be very small and shrunk to zero in the limiting process. The crack surfaces Γ_c^+ and Γ_c^- are assumed to be traction-free and electrically insulating, i.e., $t_i = \sigma_{ij}n_j = 0$ and $D_n = 0$, and the crack is parallel to the x_1-axis of the local Cartesian coordinate system. Then, Eq. 25 can be written as

$$\begin{aligned}\lim_{\varepsilon\to 0}\int_{\Gamma_\varepsilon}\left(W\delta_{jm} - \sigma_{ij}u_{i,m} - D_j E_m\right)n_j\mathrm{d}\Gamma &= \int_{\Gamma_0}\left(W\delta_{jm} - \sigma_{ij}u_{i,m} - D_j E_m\right)n_j\mathrm{d}\Gamma \\ &+ \int_{\Gamma_c^+}\left[W^+ - W^-\right]\delta_{2m}\mathrm{d}\Gamma \\ &- \lim_{\varepsilon\to 0}\int_{\Omega-\Omega_\varepsilon}\left(X_i - \rho\ddot{u}_i\right)u_{i,m}\mathrm{d}\Omega \\ &+ \lim_{\varepsilon\to 0}\int_{\Omega-\Omega_\varepsilon} RE_m\mathrm{d}\Omega \\ &- \lim_{\varepsilon\to 0}\int_{\Omega-\Omega_\varepsilon}(W_{,m})_{\exp l}\,\mathrm{d}\Omega.\end{aligned} \tag{26}$$

The left hand side of Eq. 26 is identical to the definition of the $\hat{J}$-integral (Pak and Herrmann 1986) for $m = 1$, which has the following form

$$\begin{aligned}J_1 = \int_{\Gamma_0}\left(W\delta_{j1} - \sigma_{ij}u_{i,1} - D_j E_1\right)n_j\mathrm{d}\Gamma &- \lim_{\varepsilon\to 0}\int_{\Omega-\Omega_\varepsilon}\left(X_i - \rho\ddot{u}_i\right)u_{i,1}\mathrm{d}\Omega \\ &+ \lim_{\varepsilon\to 0}\int_{\Omega-\Omega_\varepsilon} RE_1\mathrm{d}\Omega \\ &- \lim_{\varepsilon\to 0}\int_{\Omega-\Omega_\varepsilon}(W_{,1})_{\exp l}\,\mathrm{d}\Omega.\end{aligned} \tag{27}$$

Consider two independent equilibrium states in an orthotropic functionally graded material (Kim and Paulino 2003). Let the state 1 corresponds to the actual state specified by the prescribed boundary conditions, and the state 2 corresponds to an auxiliary state. Superposition of the actual and the auxiliary fields leads to another equilibrium state (state—s) for which the J-integral is given as

$$J^{(s)} = \int_{\Gamma_0} \left[\frac{1}{2}\left(\sigma_{ij}+\sigma_{ij}^{(2)}\right)\left(\varepsilon_{ij}+\varepsilon_{ij}^{(2)}\right) n_1 - (\sigma_{ij}+\sigma_{ij}^{(2)}) n_j (u_{i,1}+u_{i,1}^{(2)}) - \left(D_j+D_j^{(2)}\right) n_j \left(E_1+E_1^{(2)}\right)\right] \mathrm{d}\Gamma - \lim_{\varepsilon\to 0} \int_{\Omega-\Omega_\varepsilon} (X_i - \rho\ddot{u}_i)\,(u_{i,1}+u_{i,1}^{(2)})\mathrm{d}\Omega + \lim_{\varepsilon\to 0} \int_{\Omega-\Omega_\varepsilon} R\left(E_1+E_1^{(2)}\right)\mathrm{d}\Omega - \lim_{\varepsilon\to 0} \int_{\Omega-\Omega_\varepsilon} \left[\frac{1}{2} c_{ijkl,1}\left(\varepsilon_{ij}+\varepsilon_{ij}^{(2)}\right)\left(\varepsilon_{kl}+\varepsilon_{kl}^{(2)}\right) - e_{ikl,1}\left(E_i+E_i^{(2)}\right)\left(\varepsilon_{kl}+\varepsilon_{kl}^{(2)}\right) - \frac{1}{2} h_{ij,1}\left(E_i+E_i^{(2)}\right)\left(E_j+E_j^{(2)}\right)\right] \mathrm{d}\Omega, \quad (28)$$

which can be conveniently decomposed into

$$J^{(s)} = J + J^{(2)} + M, \quad (29)$$

where

$$J^{(2)} = \int_{\Gamma_0} \left[\frac{1}{2}\sigma_{ij}^{(2)}\varepsilon_{ij}^{(2)} n_1 - \sigma_{ij}^{(2)} n_j u_{i,1}^{(2)} - D_j^{(2)} n_j E_1^{(2)}\right] \mathrm{d}\Gamma - \lim_{\varepsilon\to 0} \int_{\Omega-\Omega_\varepsilon} \left[\frac{1}{2} C_{ijkl,1}\varepsilon_{kl}^{(2)}\varepsilon_{ij}^{(2)} - e_{ikl,1}E_i^{(2)}\varepsilon_{kl}^{(2)} - \frac{1}{2} h_{ij,1}E_i^{(2)}E_j^{(2)}\right] \mathrm{d}\Omega. \quad (30)$$

The interaction integral M is then given by

$$M = \int_{\Gamma_0} \left[\frac{1}{2}\left(\sigma_{ij}\varepsilon_{ij}^{(2)} + \sigma_{ij}^{(2)}\varepsilon_{ij}\right) n_1 - (\sigma_{ij} n_j u_{i,1}^{(2)} + \sigma_{ij}^{(2)} n_j u_{i,1}) - D_j n_j E_1^{(2)} - D_j^{(2)} n_j E_1\right] \mathrm{d}\Gamma - \lim_{\varepsilon\to 0} \int_{\Omega-\Omega_\varepsilon} (X_i - \rho\ddot{u}_i)\, u_{i,1}^{(2)} \mathrm{d}\Omega + \lim_{\varepsilon\to 0} \int_{\Omega-\Omega_\varepsilon} R E_1^{(2)} \mathrm{d}\Omega - \lim_{\varepsilon\to 0} \int_{\Omega-\Omega_\varepsilon} \left[\frac{1}{2} c_{ijkl,1}\left(\varepsilon_{ij}\varepsilon_{kl}^{(2)} + \varepsilon_{ij}^{(2)}\varepsilon_{kl}\right) - e_{ikl,1}\left(E_i\varepsilon_{kl}^{(2)} + E_i^{(2)}\varepsilon_{kl}\right) - \frac{1}{2} h_{ij,1}\left(E_i E_j^{(2)} + E_i^{(2)} E_j\right)\right] \mathrm{d}\Omega. \quad (31)$$

The electromechanical J-integral can be expressed in terms of the SIF and the EDIF (Pak 1990; Enderlein et al. 2005)

$$J = \frac{1}{2} K_M K_N Y_{MN}. \quad (32)$$

If the poling direction of the material and the mechanical loading are perpendicular to the crack, only the mode I and IV is occurring. Then, the Irwin matrix Y_{MN}has a simple form and one can write (Enderlein et al. 2005)

$$J = \frac{K_I K_I}{c_T} - \frac{K_{IV} K_{IV}}{\kappa} + \frac{K_I K_{IV}}{e}. \quad (33)$$

For two admissible fields (actual and auxiliary) one obtains

$$J^{(s)} = \frac{1}{c_T}\left(K_I+K_I^{(2)}\right)^2 + \frac{1}{e}\left(K_I+K_I^{(2)}\right)\left(K_{IV}+K_{IV}^{(2)}\right) + \frac{1}{\kappa}\left(K_{IV}+K_{IV}^{(2)}\right)^2 = J + J^{(2)} + M,$$

where

$$J^{(2)} = \frac{1}{c_T}\left(K_I^{(2)}\right)^2 + \frac{1}{e} K_I^{(2)} K_{IV}^{(2)} + \frac{1}{\kappa}\left(K_{IV}^{(2)}\right)^2,$$

and

$$M = \frac{2}{c_T} K_I K_I^{(2)} + \frac{1}{e}\left(K_I K_{IV}^{(2)} + K_I^{(2)} K_{IV}\right) + \frac{2}{\kappa} K_{IV} K_{IV}^{(2)}. \quad (34)$$

The mode-I and the mode-IV intensity factors are evaluated by solving the following system of linear algebraic equations

$$\frac{2}{c_T} K_I + \frac{1}{e} K_{IV} = M^I, \quad (35)$$

$$\frac{1}{e} K_I + \frac{2}{\kappa} K_{IV} = M^{IV}, \quad (36)$$

resulting from Eq. 34 by taking $K_I^{(2)} = 1$, $K_{IV}^{(2)} = 0$ for M^I, and $K_I^{(2)} = 0$, $K_{IV}^{(2)} = 1$ for M^{IV}, respectively. The values $M^I$and $M^{IV}$are computed numerically by Eq. 31 with an adequate choice of the auxiliary solutions according to Eq. 19.

4 Local boundary integral equations for 2D problems

Let us consider a linear transient dynamic piezoelectric problem in a continuously nonhomogeneous domain

Ω bounded by the boundary Γ and described by the governing Eqs. 1 and 2 within the quasi-static approximation for the electrical field. The following boundary and initial conditions are assumed for the mechanical quantities

$$u_i(\mathbf{x}, t) = \tilde{u}_i(\mathbf{x}, t) \quad \text{on } \Gamma_u,$$

$$t_i(\mathbf{x}, t) = \tilde{t}_i(\mathbf{x}, t) \quad \text{on } \Gamma_t,$$

$$u_i(\mathbf{x}, t)|_{t=0} = u_i(\mathbf{x}, 0) \quad \text{and}$$

$$\dot{u}_i(\mathbf{x}, t)|_{t=0} = \dot{u}_i(\mathbf{x}, 0) \text{ in } \Omega,$$

and for electrical ones

$$\psi(\mathbf{x}) = \tilde{\psi}(\mathbf{x}) \text{ on } \Gamma_p,$$

$$n_i D_i(\mathbf{x}) = \tilde{Q}(\mathbf{x}) \text{ on } \Gamma_q,$$

where Γ_u is the part of the global boundary with prescribed displacements, and on Γ_t, Γ_p and Γ_q the traction vector, the electric potential and the surface density of free charge are prescribed, respectively. It is noted that $\Gamma_u + \Gamma_t = \Gamma_p + \Gamma_q$.

Applying the Laplace-transform to the governing equations we obtain

$$\bar{\sigma}_{ij,j}(\mathbf{x}, p) - \rho(\mathbf{x}) p^2 \bar{u}_i(\mathbf{x}, p) = -\bar{F}_i(\mathbf{x}, p), \tag{37}$$

where p is the Laplace-transform parameter, and

$$\bar{F}_i(\mathbf{x}, p) = \bar{X}_i(\mathbf{x}, p) + p u_i(\mathbf{x}, 0) + \dot{u}_i(\mathbf{x}, 0).$$

Instead of writing the global weak-form for the above governing equations, we apply the MLPG method to construct a weak-form over the local fictitious subdomains such as Ω_s, which is a small region taken for each node inside the global domain (Atluri 2004). The local subdomains overlap each other, and cover the whole global domain Ω. The local subdomains could be of any geometrical shape and size. In the present paper, the local subdomains are taken to be of circular shape. The local weak-form of the governing Eq. 37 can be written as

$$\int_{\Omega_s} \left[\bar{\sigma}_{ij,j}(\mathbf{x}, p) - \rho(\mathbf{x}) p^2 \bar{u}_i(\mathbf{x}, p) + \bar{F}_i(\mathbf{x}, p) \right] \times u^*_{ik}(\mathbf{x}) d\Omega = 0, \tag{38}$$

where $u^*_{ik}(\mathbf{x})$is a test function.
Using

$$\bar{\sigma}_{ij,j} u^*_{ik} = \left(\bar{\sigma}_{ij} u^*_{ik}\right)_{,j} - \bar{\sigma}_{ij} u^*_{ik,j}$$

and applying the Gauss divergence theorem one can write

$$\int_{\partial\Omega_s} \bar{\sigma}_{ij}(\mathbf{x}, p) n_j(\mathbf{x}) u^*_{ik}(\mathbf{x}) d\Gamma - \int_{\Omega_s} \bar{\sigma}_{ij}(\mathbf{x}, p) u^*_{ik,j}(\mathbf{x}) d\Omega + \int_{\Omega_s} \left[\bar{F}_i(\mathbf{x}, p) - \rho(\mathbf{x}) p^2 \bar{u}_i(\mathbf{x}, p) \right] u^*_{ik}(\mathbf{x}) d\Omega = 0, \tag{39}$$

where $\partial\Omega_s$ is the boundary of the local subdomain which consists of three parts $\partial\Omega_s = L_s \cup \Gamma_{st} \cup \Gamma_{su}$ (Atluri 2004). It is noted that L_s is the local boundary that is totally inside the global domain, Γ_{st} is the part of the local boundary which coincides with the global traction boundary, i.e., $\Gamma_{st} = \partial\Omega_s \cap \Gamma_t$, and similarly Γ_{su} is the part of the local boundary that coincides with the global displacement boundary, i.e., $\Gamma_{su} = \partial\Omega_s \cap \Gamma_u$.

By choosing a Heaviside step function as the test function $u^*_{ik}(\mathbf{x})$ in each subdomain

$$u^*_{ik}(\mathbf{x}) = \begin{cases} \delta_{ik} & \text{at } \mathbf{x} \in \Omega_s \\ 0 & \text{at } \mathbf{x} \notin \Omega_s \end{cases}$$

the local weak-form (39) is then converted into the following local boundary-domain integral equations

$$\int_{L_s + \Gamma_{su}} \bar{t}_i(\mathbf{x}, p) d\Gamma - \int_{\Omega_s} \rho(\mathbf{x}) p^2 \bar{u}_i(\mathbf{x}, p) d\Omega = -\int_{\Gamma_{st}} \bar{\tilde{t}}_i(\mathbf{x}, p) d\Gamma - \int_{\Omega_s} \bar{F}_i(\mathbf{x}, p) d\Omega. \tag{40}$$

Note that the local integral Eq. 40 is valid for both homogeneous and nonhomogeneous linear piezoelelectric solids. Nonhomogeneous material properties are included in Eq. 40 through the elastic and the piezoelectric tensors of material coefficients in the traction components.

Similarly, the local weak-form of the governing Eq. 2 in the Laplace transformed domain is given by

$$\int_{\Omega_s} \left[\bar{D}_{j,j}(\mathbf{x}, p) - \bar{R}(\mathbf{x}, p) \right] v^*(\mathbf{x}) d\Omega = 0, \tag{41}$$

where $v^*(\mathbf{x})$ is a test function.

Applying the Gauss divergence theorem to the local weak-form and considering the Heaviside step function for the test function $u^*(\mathbf{x})$, one obtains

$$\int_{L_s+\Gamma_{sp}} \bar{Q}(\mathbf{x}, p)d\Gamma = -\int_{\Gamma_{sq}} \tilde{\bar{Q}}(\mathbf{x}, p)d\Gamma + \int_{\Omega_s} \bar{R}(\mathbf{x}, p)d\Omega, \tag{42}$$

where

$$\bar{Q}(\mathbf{x}, p) = \bar{D}_j(\mathbf{x}, p)n_j = \left[e_{jkl}\bar{u}_{k,l}(\mathbf{x}, p) - h_{jk}\bar{\psi}_{,k}(\mathbf{x}, p)\right]n_j.$$

In the MLPG method the test and the trial functions are not necessarily from the same functional spaces. For internal nodes, the test function is chosen as the Heaviside step function with its support on the local subdomain. The trial functions, on the other hand, are chosen to be the moving least-squares (MLS) approximation over a number of nodes spread within the domain of influence. The approximated functions for the Laplace transforms of the mechanical displacements and the electric potential can be written as (Atluri 2004)

$$\bar{\mathbf{u}}^h(\mathbf{x}, p) = \mathbf{\Phi}^T(\mathbf{x}) \cdot \hat{\mathbf{u}}(p) = \sum_{a=1}^{n} \phi^a(\mathbf{x})\hat{\mathbf{u}}^a(p),$$

$$\bar{\psi}^h(\mathbf{x}, p) = \sum_{a=1}^{n} \phi^a(\mathbf{x})\hat{\psi}^a(p), \tag{43}$$

where the nodal values $\hat{\mathbf{u}}^a(p)$ and $\hat{\psi}^a(p)$ are fictitious parameters for the displacements and the electric potential, respectively and $\phi^a(\mathbf{x})$ is the shape function associated with the node a. The number of nodes n used for the approximation is determined by the weight function $w^a(\mathbf{x})$. A 4^{th} order spline-type weight function is applied in the present work

$$w^a(\mathbf{x}) = \begin{cases} 1 - 6\left(\frac{d^a}{r^a}\right)^2 + 8\left(\frac{d^a}{r^a}\right)^3 \\ -3\left(\frac{d^a}{r^a}\right)^4 \quad 0 \le d^a \le r^a \\ 0, \qquad\qquad d^a \ge r^a \end{cases}, \tag{44}$$

where $d^a = \|\mathbf{x} - \mathbf{x}^a\|$ and r^a is the size of the support domain. It is seen that the C^1-continuity is ensured over the entire domain, therefore the continuity conditions of the tractions and the electric charge are satisfied.

The Laplace transform of the traction vectors $\bar{t}_i(\mathbf{x}, p)$ at a boundary point $\mathbf{x} \in \partial\Omega_s$ are approximated in terms of the same nodal values $\hat{\mathrm{u}}^a(p)$ as

$$\bar{\boldsymbol{t}}^h(\mathbf{x}, p) = \mathbf{N}(\mathbf{x})\mathbf{C}(\mathbf{x})\sum_{a=1}^{n} \mathbf{B}^a(\mathbf{x})\hat{\mathrm{u}}^a(p) + \mathbf{N}(\mathbf{x})\mathbf{L}(\mathbf{x})\sum_{a=1}^{n} \mathbf{P}^a(\mathbf{x})\hat{\psi}^a(p), \tag{45}$$

where the matrix $\mathbf{N}(\mathbf{x})$ is related to the normal vector $\mathbf{n}(\mathbf{x})$ on $\partial\Omega_s$ by

$$\mathbf{N}(\mathbf{x}) = \begin{bmatrix} n_1 & 0 & n_2 \\ 0 & n_2 & n_1 \end{bmatrix},$$

and the matrices $\mathbf{B}^a$ and $\mathbf{P}^a$ are represented by the gradients of the shape functions as

$$\mathbf{B}^a(\mathbf{x}) = \begin{bmatrix} \phi^a_{,1} & 0 \\ 0 & \phi^a_{,2} \\ \phi^a_{,2} & \phi^a_{,1} \end{bmatrix}, \quad \mathbf{P}^a(\mathbf{x}) = \begin{bmatrix} \phi^a_{,1} \\ \phi^a_{,2} \end{bmatrix}.$$

Similarly the Laplace transform of the electrical charge $\bar{Q}(\mathbf{x}, p)$ can be approximated by

$$\bar{Q}^h(\mathbf{x}, p) = \mathbf{N}_1(\mathbf{x})\mathbf{G}(\mathbf{x})\sum_{a=1}^{n} \mathbf{B}^a(\mathbf{x})\hat{\mathbf{u}}^a(p) - \mathbf{N}_1(\mathbf{x})\mathbf{H}(\mathbf{x})\sum_{a=1}^{n} \mathbf{P}^a(\mathbf{x})\hat{\psi}^a(p), \tag{46}$$

where the matrices $\mathbf{G}$ and $\mathbf{H}$ are defined in Eq. 9 and

$$\mathbf{N}_1(\mathbf{x}) = \begin{bmatrix} n_1 & n_2 \end{bmatrix}.$$

Obeying the boundary conditions at those nodal points on the global boundary, where the displacements and the electrical potential are prescribed, and making use of the approximation formula (43), one obtains the discretized form of the boundary conditions as

$$\sum_{a=1}^{n} \phi^a(\boldsymbol{\zeta})\hat{\mathbf{u}}^a(p) = \tilde{\bar{\mathbf{u}}}(\boldsymbol{\zeta}, p) \quad \text{for } \boldsymbol{\zeta} \in \Gamma_u, \tag{47}$$

$$\sum_{a=1}^{n} \phi^a(\boldsymbol{\zeta})\hat{\psi}^a(p) = \tilde{\bar{\psi}}(\boldsymbol{\zeta}, p) \quad \text{for } \boldsymbol{\zeta} \in \Gamma_p. \tag{48}$$

Furthermore, in view of the MLS-approximation (45) and (46) for the unknown quantities in the local boundary-domain integral Eqs. 40 and 42, we obtain their discretized forms as

$$\sum_{a=1}^{n}\left(\int_{L_s+\Gamma_{su}} \mathbf{N}(\mathbf{x})\mathbf{C}(\mathbf{x})\mathbf{B}^a(\mathbf{x})d\Gamma - \rho(\mathbf{x})p^2\int_{\Omega_s} \phi^a(\mathbf{x})d\Omega\right)\hat{\mathbf{u}}^a(p) + \sum_{a=1}^{n}\left(\int_{L_s+\Gamma_{su}} \mathbf{N}(\mathbf{x})\mathbf{L}(\mathbf{x})\mathbf{P}^a(\mathbf{x})d\Gamma\right)\hat{\psi}^a(p) = -\int_{\Gamma_{st}} \tilde{\bar{\boldsymbol{t}}}(\mathbf{x}, p)d\Gamma - \int_{\Omega_s} \bar{F}(\mathbf{x}, p)d\Omega, \tag{49}$$

$$\sum_{a=1}^{n}\left(\int\limits_{L_s+\Gamma_{sp}} \mathbf{N}_1(\mathbf{x})\mathbf{G}(\mathbf{x})\mathbf{B}^a(\mathbf{x})d\Gamma\right)\hat{\mathbf{u}}^a(p)$$
$$-\sum_{a=1}^{n}\left(\int\limits_{L_s+\Gamma_{sp}} \mathbf{N}_1(\mathbf{x})\mathbf{H}(\mathbf{x})\mathbf{P}^a(\mathbf{x})d\Gamma\right)\hat{\psi}^a(p)$$
$$=-\int\limits_{\Gamma_{sq}}\tilde{\tilde{Q}}(\mathbf{x},p)d\Gamma+\int\limits_{\Omega_s}\bar{R}(\mathbf{x},p)d\Omega, \qquad (50)$$

which are considered on the sub-domains adjacent to interior nodes as well as to the boundary nodes on Γ_{st} and Γ_{sq}.

5 Numerical examples

5.1 A central crack in a finite homogeneous strip

In the first example a straight central crack in a homogeneous finite strip under a uniform pure mechanical and/or electrical displacement is analyzed (Fig. 2). The strip is subjected to an impact load with Heaviside time variation and the intensity$\sigma_0 = 1\,\text{Pa}$ for a pure mechanical load and $D_0 = 1\,\text{Cm}^{-2}$ for a pure electrical load, respectively. Homogeneous material properties are selected to test the present computational method. The material coefficients of the strip correspond to the PZT-4 material and they are given by

$$c_{11} = 13.9\cdot 10^{10}\,\text{Nm}^{-2},\quad c_{12} = 7.43\cdot 10^{10}\,\text{Nm}^{-2},$$
$$c_{22} = 11.5\cdot 10^{10}\,\text{Nm}^{-2},\quad c_{44} = 2.56\cdot 10^{10}\,\text{Nm}^{-2},$$

$$e_{15} = 12.7\,\text{Cm}^{-2},\quad e_{21} = -5.2\,\text{Cm}^{-2},$$
$$e_{22} = 15.1\,\text{Cm}^{-2},$$

$$h_{11} = 6.46\cdot 10^{-9}\,\text{C(Vm)}^{-1},$$
$$h_{22} = 5.62\cdot 10^{-9}\,\text{C(Vm)}^{-1},\quad \rho = 7,500\,\text{kg/m}^3.$$

The strip width $w = 1.25a$, crack length $2a = 1.0\,\text{m}$ and height of the strip $h = 1.2w$ are considered. Due to the symmetry of the problem with respect to the crack line, only a quarter of the specimen is numerically analyzed. The mechanical displacement and the electrical potential fields in the quarter of the specimen are approximated by using 930 (31×30) nodes equidistantly distributed. The local subdomains are considered to be circular with a radius $r_{loc} = 0.028\,\text{m}$. The integration path Γ_0 for the evaluation of the M-integrals

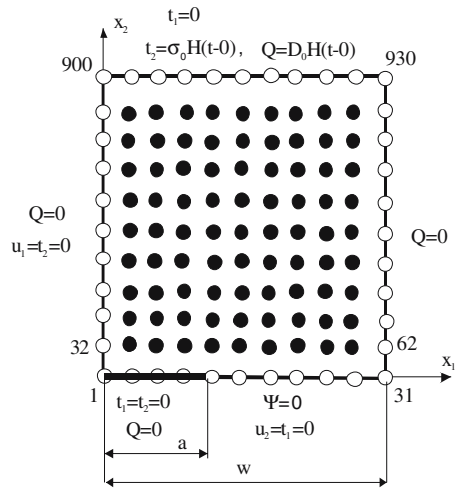

Fig. 2 Central crack in a finite homogeneous strip

has a rectangular shape with a size $0.75\times0.75\,\text{m}$ and the crack-tip being at the centre of this area. To test the accuracy of the proposed method, an additional integration path with a size $0.9\times0.9\,\text{m}$ has also been used for evaluating the fracture parameters. The discrepancies of the numerical values obtained for these fracture parameters from the two paths were less than 1%.

The normalized stress intensity factor K_I/K_I^{stat} and electrical displacement factor $\Lambda K_{IV}/K_I^{stat}$ are compared with FEM results in Figs. 3 and 4, where $K_I^{stat} = 1.4\,\text{Pa}\cdot\text{m}^{1/2}$ for the considered geometry and load, and $\Lambda = e_{22}/h_{22}$. FEM results are obtained by the ANSYS-code with 8,037 quadratic (8-node) elements (plane223) and 2,000 time steps.

One can observe a quite good agreement of FEM and present results in both figures. The dynamic value of the SIF is approximately doubled with respect to the static one. The electrical displacement intensity factor for a pure static mechanical load is vanishing (Sladek et al. 2007). Contrary to the static case the EDIF is not vanishing in the dynamic case with a finite velocity of wave propagation for a pure mechanical load (Fig. 4).

The SIF and the EDIF for a pure electrical displacement load are presented in Fig. 5. Intensity factors are normalized by the same way like in the previous figures. Also in this case, contrary to the static case, the SIF is not vanishing. From the Maxwell's equations, it is known that the velocity of electromagnetic waves is equal to the speed of light, which is much greater than the velocity of elastic waves. Hence, the use of quasi-

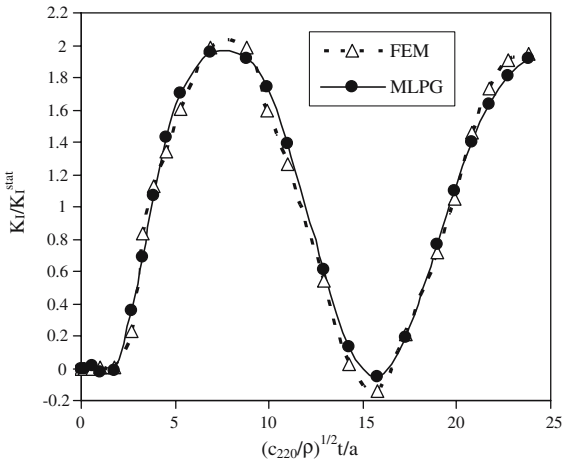

Fig. 3 Normalized stress intensity factor for a central crack in a strip under a pure mechanical load σ_0

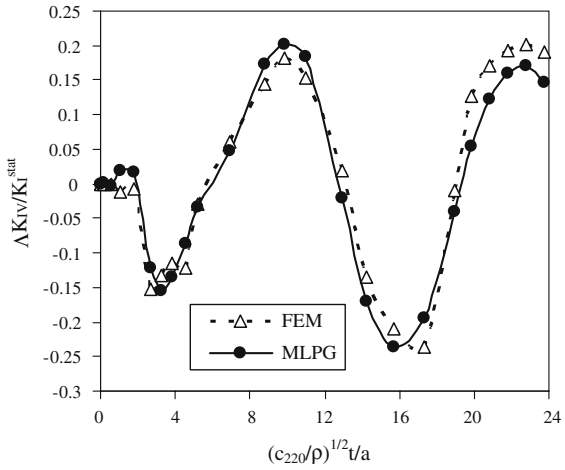

Fig. 4 Normalized electrical displacement intensity factor for a central crack in a strip under a pure mechanical load σ_0

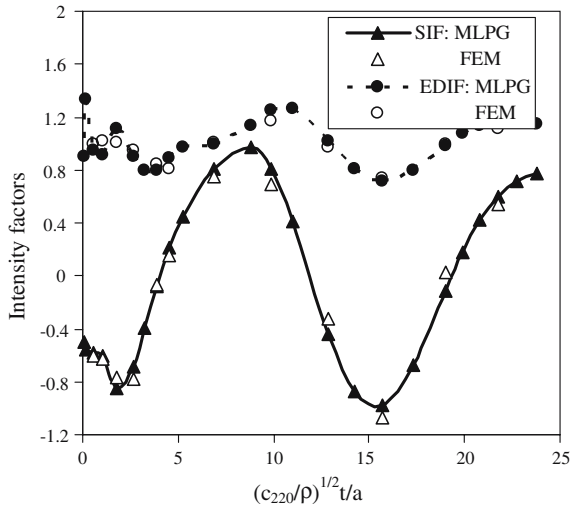

Fig. 5 Normalized intensity factors for a central crack in a strip under a pure electrical displacement load D_0

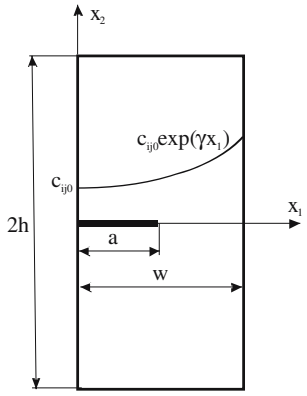

Fig. 6 An edge crack in a finite strip with graded material properties in x_1

static approximation in Eqs. 1 and 2 is justified for the interaction of electrical and mechanical fields. The response of the electric fields is immediate, while that of the elastic ones is taken as finite because of the finite velocity of elastic waves. On the other hand, in a static case, the response of both the mechanical (strain, stress) and electrical fields is immediate. Thus, the SIF is vanishing in such a case since the stresses σ_{22} are zero ahead the crack tip on the crack line because of the immediate electromechanical interaction. In the dynamic case the stress field is coupled not only to the immediate electric field, but also to inertia forces (Enderlein et al. 2005).

5.2 An edge crack in a finite FGPM strip

An edge crack in a finite strip is analyzed in the second example. The sample geometry is given in Fig. 6 with following values: $a = 0.5$, $a/w = 0.4$ and $h/w = 1.2$. Due to the symmetry with respect to x_1 only a half of the specimen is modeled. We have used 930 nodes equidistantly distributed for the MLS approximation of physical fields. On the top of the strip a uniform impact tension σ_0 and electrical displacement D_0 (Heaviside time variation) are applied, respectively.

Functionally graded material properties in x_1 coordinate are considered. An exponential variation for the

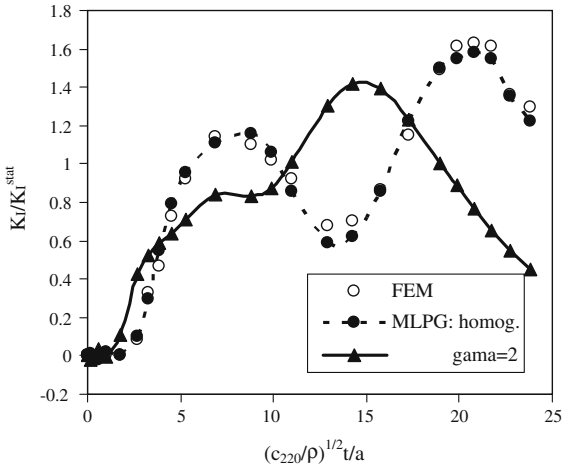

Fig. 7 Influence of the material gradation on the stress intensity factor in a cracked strip under a pure mechanical impact load $\sigma_0 H(t-0)$

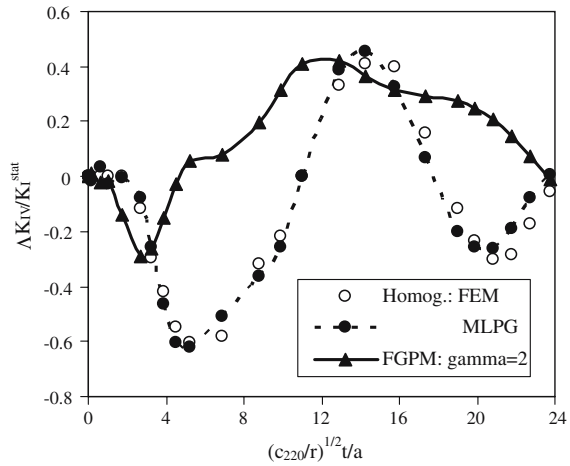

Fig. 8 Influence of the material gradation on the EDIF in the cracked strip under a pure mechanical impact load $\sigma_0 H(t-0)$

elastic, piezoelectric and dielectric tensors is used

$$c_{ijkl}(\mathbf{x}) = c_{ijkl0}\exp(\gamma x_1),$$

$$e_{ijk}(\mathbf{x}) = e_{ijk0}\exp(\gamma x_1)$$

$$h_{ij}(\mathbf{x}) = h_{ij0}\exp(\gamma x_1), \tag{51}$$

where c_{ijkl0}, e_{ijk0} and h_{ij0} correspond to parameters used in the previous example.

The influence of the material gradation on the stress intensity factor and electrical displacement intensity factor is analyzed. The temporal variation of the SIF and the EDIF in the cracked strip under a pure mechanical load is presented in Figs. 7 and 8, respectively. The static stress intensity factor for the considered load and geometry is equal to $K_I^{stat} = 2.642\,\mathrm{Pa}\cdot\mathrm{m}^{1/2}$. Numerical results for a homogeneous strip are compared with FEM ones, and a quite good agreement is observed.

For a gradation of mechanical material properties with x_1 coordinate and a uniform mass density, the wave propagation is growing with x_1. Therefore, the peak value of the SIF is reached in a shorter time instant in FGPM strip than in a homogeneous one. The maximum value of the SIF is only slightly reduced for the FGPM cracked strip.

Next, the cracked strip under a pure electrical displacement impact load is analyzed. Since static SIF and EDIF are uncoupled it has to valid $K_{IV}^{stat} = K_I^{stat}$. The temporal variation of the EDIF is given in Fig. 9. The EDIF is significantly reduced for a cracked FGPM compared to a homogeneous strip. The oscillation of

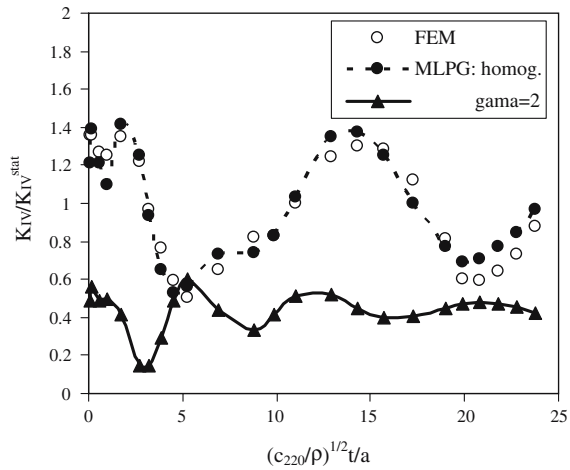

Fig. 9 Temporal variation of the EDIF in the cracked strip under a pure electrical displacement impact load $D_0 H(t-0)$

amplitudes for EDIF is again faster in an FGPM strip. Similar phenomena are observed for SIF in Fig. 10.

The influence of the specimen height on the normalized dynamic stress intensity factor in a homogeneous cracked strip under a pure mechanical impact load is observed in Fig. 11. For a larger specimen height a reduced oscillation of the stress intensity factor is occurred. A longer sleeping time of the SIF for a larger specimen is due to larger distance from the applied place to the crack tip.

When cracks in piezoelectric solids are investigated, an important question is how to prescribe electric boundary conditions on the crack-surfaces. For completely

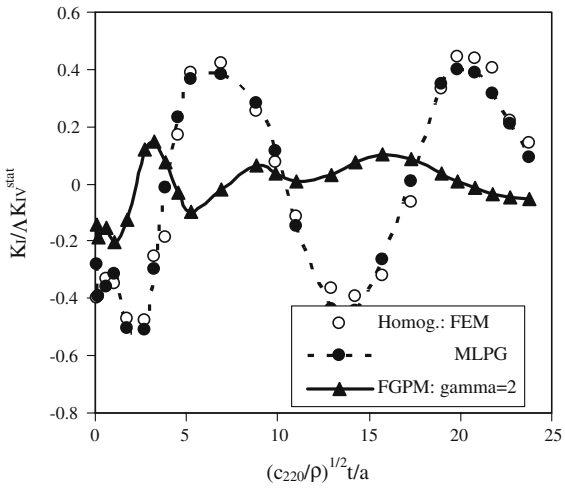

Fig. 10 Temporal variation of the SIF in the cracked strip under a pure electrical displacement impact load $D_0 H(t-0)$

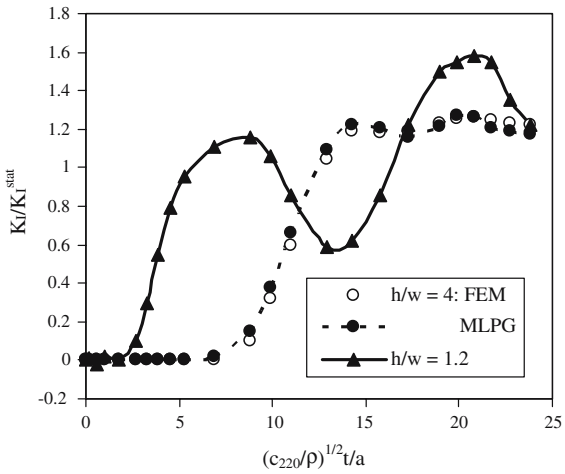

Fig. 11 Influence of the specimen height on the SIF in a homogeneous cracked strip under a pure mechanical impact load $\sigma_0 H(t-0)$

permeable conditions

$$\psi^+ = \psi^-, \quad D_n^+ = D_n^-,$$

the crack is not visible for the electric field. Contrary, completely impermeable boundary conditions lead to vanishing electrical displacements

$$D_n^+ = D_n^- = 0.$$

Realistic electrical boundary conditions are between the above mentioned two extreme cases. The dielectric property of the medium inside the crack is described by constants $h = \mathbf{h}_r \cdot \mathbf{h}_0$, where $\mathbf{h}_0$is the permittivity of the vacuum inside the crack and $\mathbf{h}_r$is a relative permittivity. The dielectric law gives

$$D_n^+ = D_n^- = -h\frac{\psi^+ - \psi^-}{u_n^+ - u_n^-}.$$

Since the mechanical displacements and the electric potential are dependent on the electric displacement, an iterative solution procedure is needed to handle this kind of electrical boundary conditions (Kuna 2006). We have used the two extreme electrical boundary conditions on the crack-surfaces. Numerical results for the normalized dynamic SIF and the normalized dynamic EDIF are given in Figs. 12 and 13, respectively. The normalized dynamic SIF remains almost the same for both the permeable and the impermeable boundary conditions in homogeneous and continuously nonhomogeneous piezoelectric solids. The variation of the normalized dynamic EDIF for permeable electrical boundary conditions is similar to the variation of the normalized dynamic SIF.

For a positive value of the gradation parameter γ of the mechanical material properties in the x_1-direction and a uniform mass density, the wave propagation velocity is growing with x_1-coordinate. Therefore, the first peak value of the dynamic SIF is reached at a shorter time instant in FGPM strip than in a homogeneous one. The maximum value of the dynamic SIF is only slightly reduced for the cracked FGPM strip compared to that of the cracked homogeneous strip.

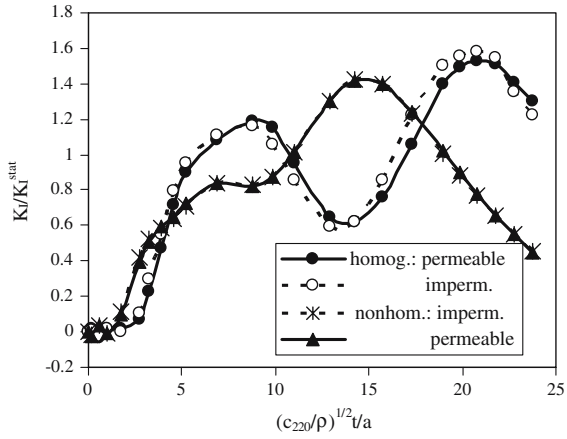

Fig. 12 Time variation of the normalized dynamic stress intensity factor

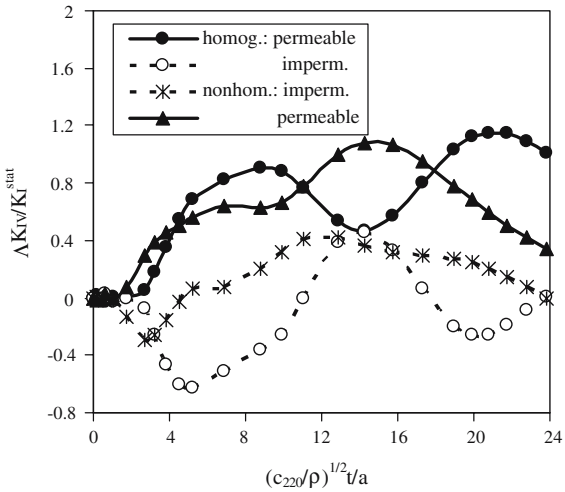

Fig. 13 Time variation of the normalized dynamic electrical displacement intensity factor

6 Conclusions

Growing application of functionally graded piezoelectric materials in many engineering structures with safety integrity put a requirement to analyze crack problems in such materials. Since problems under a transient dynamic load are unsolved in literature the first attempt is given in the present paper. For this purpose a meshless local Petrov-Galerkin method (MLPG) is developed in continuously nonhomogeneous bodies under a transient dynamic load. The analyzed 2-D domain is divided into small overlapping circular subdomains. A unit step function is used as the test functions in the local weak-form. The derived local boundary-domain integral equations are nonsingular. The moving least-squares (MLS) scheme is adopted for approximating the physical quantities. The proposed method is a truly meshless method, which requires neither domain elements nor background cells in either the interpolation or the integration. It is shown that the asymptotic fields in the crack-tip vicinity in a continuously nonhomogeneos medium is the same as in a homogeneous one. A contour integral method is developed for the computation of stress and electric intensity factors. The results in numerical examples show a strong dependence of the stress intensity factor and electrical displacement intensity factor even such dynamical cases where no coupling is observed for a static load. An impact load is leading to a dynamic overshoot of the static intensity factors. A gradation of material properties affects both intensity factors.

Acknowledgements The authors acknowledge the support by the Slovak Science and Technology Assistance Agency registered under number APVV-51-021205, APVT-20-035404, the Slovak Grant Agency VEGA-2/6109/6, and the German Research Foundation (DFG) under the project number ZH 15/6-1.

References

Atluri SN (2004) The meshless method, (MLPG) for domain & BIE discretizations. Tech Science Press

Atluri SN, Han ZD, Shen S (2003) Meshless local Petrov-Galerkin (MLPG) approaches for solving the weakly-singular traction & displacement boundary integral equations. CMES: Comp Modeling Eng Sci 4:507–516

Atluri SN, Liu HT, Han ZD (2006) Meshless local Petrov-Galerkin (MLPG) mixed finite difference method for solid mechanics. CMES: Comp Modeling Eng Sci 15:1–16

Belytschko T, Krogauz Y, Organ D, Fleming M, Krysl P (1996) Meshless methods; an overview and recent developments. Comp Meth Appl Mech Eng 139:3–47

Chen J, Liu ZX, Zou ZZ (2003) Electromechanical impact of a crack in a functionally graded piezoelectric medium. Theor Appl Fract Mech 39:47–60

Chen WQ, Lu Y, Ye GR, Cai JB (2002) 3D electrostatic fields in a functionally graded piezoceramic hollow sphere under mechanical and electric loading. Arch Appl Mech 72:39–51

Davi G, Milazzo A (2001) Multidomain boundary integral formulation for piezoelectric materials fracture mechanics. Int J Solids Struct 38:2557–2574

Eischen JW (1987) Fracture of nonhomogeneous materials. Int J Fract 34:3–22

Enderlein M, Ricoeur A, Kuna M (2005) Finite element techniques for dynamic crack analysis in piezoelectrics.. Int J Fract 134:191–208

Garcia-Sanchez F, Saez A, Dominguez J (2005) Anisotropic and piezoelectric materials fracture analysis by BEM. Comp Struct 83:804–820

Garcia-Sanchez F, Zhang Ch, Sladek J, Sladek V (2007) 2-D transient dynamic crack analysis in piezoelectric solids by BEM. Comput Mater Sci 39:179–186

Govorukha V, Kamlah M (2004) Asymptotic fields in the finite element analysis of electrically permeable interfacial cracks in piezoelectric bimaterials. Arch Appl Mech 74:92–101

Gruebner O, Kamlah M, Munz D (2003) Finite element analysis of cracks in piezoelectric materials taking into account the permittivity of the crack medium. Eng Fract Mech 70:1399–1413

Gross D, Rangelov T, Dineva P (2005) 2D wave scattering by a crack in a piezoelectric plane using traction BIEM. SID: Struct Integrity Durability 1:35–47

Han F, Pan E, Roy AK, Yue ZQ (2006) Responses of piezoelectric, transversaly isotropic, functionally graded and multilayered half spaces to uniform circular surface loading. CMES: Comp Modeling Eng Sci 14:15–30

Jin ZH, Noda N (1994) Crack-tip singular fields in nonhomogeneous materials. ASME J Appl Mech 61:738–740

Kim JH, Paulino GH (2003) The interaction integral for fracture of orthotropic functionally graded materials: evaluation of stress intensity factors. Int J Solids Struct 40:3967–4001

Kuna M (1998) Finite element analyses of crack problems in piezoelectric structures. Comput Mater Sci 13:67–80

Kuna M (2006) Finite element analyses of cracks in piezoelectric structures—a survey. Arch Appl Mech 76:725–745

Li C, Weng GJ (2002a) Antiplane crack problem on functionally graded piezoelectric materials. ASME J Appl Mech 69:481–488

Li C, Weng GJ (2002b) Yoffe-type moving crack in a functionally graded piezoelectric material. Proc Roy Soc Lond A 458:381–399

Liu GR, Dai KY, Lim KM, Gu YT (2002) A point interpolation mesh free method for static and frequency analysis of two-dimensional piezoelectric structures. Comput Mech 29:510–519

Ohs RR, Aluru NR (2001) Meshless analysis of piezoelectric devices. Comput Mech 27:23–36

Pan E (1999) A BEM analysis of fracture mechanics in 2D anisotropic piezoelectric solids. Eng Anal Boundary Elements 23:67–76

Pak YE (1990) Crack extension force in a piezoelectric material. ASME J Appl Mech 57:647–653

Pak YE (1992) Linear electro-elastic fracture mechanics of piezoelectric materials. Int J Fract 54:79–100

Pak YE, Herrmann CT (1986) Conservation laws and the material momentum tensor for the elastic dielectric. Int J Eng Sci 24:1365–1374

Park SB, Sun CT (1995) Effect of electric field on fracture of piezoelectric ceramics. Int J Fract 70:203–216

Parton VZ, Kudryavtsev BA (1988) Electromagnetoelasticity, Piezoelectrics and Electrically Conductive Solids. Gordon and Breach Science Publishers, New York

Paulino GH, Jin ZH, Dodds RH (2003) Failure of functionally graded materials. In: Karihaloo B, Knauss WG (eds), Comprehensive structural integrity, vol 2. Elsevier Science, pp 607–644

Ricoeur A, Kuna M. (2003) Influence of electric fields on the fracture of ferroelectric ceramics. J Eur Ceram Soc 23:1313–1328

Sheng N, Sze KY (2006) Multi-region Trefftz boundary element method for fracture analysis in plane piezoelectricity. Comput Mech 37:381–393

Shindo Y, Narita F, Tanaka K (1996) Electroelastic intensification near anti-plane shear crack in orthotropic piezoelectric ceramic strip. Theor Appl Fract Mech 25:65–71

Shindo Y, Tanaka K, Narita F (1997) Singular stress and electric fields of a piezoelectric ceramic strip with a finite crack under longitudinal shear. Acta Mechanica 120:31–45

Sladek J, Sladek V, Atluri SN (2004) Meshless local Petrov-Galerkin method in anisotropic elasticity. CMES: Comp Modeling Eng Sci 6:477–489

Sladek J, Sladek V, Zhang Ch, Garcia-Sanchez F, Wunsche M (2006) Meshless local Petrov-Galerkin method for plane piezoelectricity. CMC: Comp Mater Continua 4:109–118

Sladek J, Sladek V, Zhang Ch, Solek P, Starek L (2007) Fracture analyses in continuously nonhomogeneous piezoelectric solids by the MLPG. CMES: Comp Modeling Eng Sci 19:247–262

Sosa H (1991) Plane problems in piezoelectric media with defects. Int J Solids Struct 28:491–505

Suresh S, Mortensen A (1998) Fundamentals of functionally graded materials. Institute of Materials, London

Ueda S (2003) Crack in functionally graded piezoelectric strip bonded to elastic surface layers under electromechanical loading. Theor Appl Fract Mech 40:225–236

Yang JH, Lee KY (2001) Penny shaped crack in a three-dimensional piezoelectric strip under in-plane normal loadings. Acta Mechanica 148:187–197

Wang BL, Noda N (2001) Thermally induced fracture of a smart functionally graded composite structure. Theor Appl Fract Mech 35:93–109

Zhu T, Zhang JD, Atluri SN (1998) A local boundary integral equation (LBIE) method in computational mechanics, and a meshless discretization approaches. Comput Mech 21:223–235

Zhu X, Wang Z, Meng A (1995) A functionally gradient piezoelectric actuator prepared by metallurgical process in PMN-PZ-PT system. J Mater Sci Lett 14:516–518

Zhu X, Zhu J, Zhou S, Li Q, Liu Z (1999) Microstructures of the monomorph piezoelectric ceramic actuators with functionally gradient. Sens Actuators A 74:198–202